An iterative time-marching scheme for the investigation of hydrodynamic interaction between multi-ships during overtaking

Mingxin Li [1], Zhi-Ming Yuan [2*], Long-bin Tao [1, 2]
1. *Department of Naval Architecture and Ocean Engineering, Jiangsu University of Science and Technology, Zhenjiang, China*
2. *Department of Naval Architecture, Ocean & Marine Engineering, University of Strathclyde, Glasgow, UK*

Abstract: An iterative time-marching scheme is developed to investigate the hydrodynamic interactions between multiple ships. Such an unsteady interactive effect could be magnified in restricted waterways, *e.g.* a channel or harbor area. To the author's knowledge, nearly all the research on the ship-to-ship interaction neglecting the free surface effects. The free surface is usually treated as a rigid wall. This assumption is only reasonable when the speed of the ships is very low in deep water condition, due to the hydrodynamic interaction between the ships is mainly induced by near-field disturbances. However, when the moving speeds are moderately higher, especially with a small lateral separation between ships, the far-field effects arising from the ship waves become important. The main objective of the present paper is to develop an iterative time-matching algorithm to solve the hydrodynamic interaction between high-speed ships taking into account the nonlinear free surface boundary condition in time domain.

Key words: Iterative time-marching scheme, hydrodynamic interaction, multi-ships, free surface

Introduction

Hydrodynamic interaction occurs when a ship is overtaking (or being overtaken) other ships. Because of the confined nature of the realistic environment, operating safety and accurate control of the vessel require the knowledge of the hydrodynamic forces acting on it. A numerical technology is developed and applied to this unsteady interaction problem for determining the magnitude of such forces or moments.

Pioneering studies have provided fundamental insight into the problem of the interaction between multiple ships since the 1960s. The slender-body theory has been widely used during the 1960s-1990s[1-6]. For the ship travelling at relatively low speed, the numerical calculations based on strip theory showed a good prediction of the force and moment on ships during the passing or overtaking process. However, due to the slender-body assumption adopted in these studies the 3D effects were not considered. Korsmeyer, Lee[7] adopted a 3D panel method for any number of arbitrarily shaped bodies. However, the model neglected the free surface effect. More recently, the three-dimensional panel method has been more commonly used[8-11]. Although they did investigated the effects of unsteady free surface waves on interaction forces, they drew the conclusion that the potential flow could provide a good prediction of interaction forces on ships travelling at relatively low speed[12]. The free surface effect is taken into accounting by researchers[13-15], the unsteadiness of the problem is handled with a quasi-steady approach, which is not properly involved in the high-speed case of the ship-to-ship problem. More recently, Ren, Xu[16] simulation the ships moving in shallow water accounting for the sinkage and trim.

With the development of computational technology, CFD (Computational Fluid Dynamics) has been used to investigate the viscous effects on the ship to ship problems by various turbulence models[17]. However, no results were made to investigate the free surface effects (or the ship-to-ship problem is treated as a steady problem). The long-time unsteady free surface waves are still not included in their research. The URANS simulations were performed by Mousaviraad, Sadat-Hosseini[18], in which the free surface boundary condition was considered. However, these studies focus more on hydrodynamic forces. The results of free surface elevation were neither measured in the model tests nor presented in the CFD simulations. Zhou, Abdelwahab[19] compared the RANS-based CFD method with scaled model experiments to investigate the hydrodynamic interactions between the passing ship-generated waves and the moored ship. The demand for computational power is a bottleneck if there are more than one ships

Biography: Mingxin Li (1989-), Male, PhD,
E-mail: mingxin.li@just.edu.cn
*** Corresponding author:** Zhi-Ming Yuan,
E-mail: zhiming.yuan@strath.ac.uk

are presented (or the distance between ship is large).

Most studies mentioned above adopted the assumptions that the encountering or overtaking speed is low or the unsteady problem is handled with a quasi-steady method. These assumptions significantly reduce the complexity of unsteady ship to ship interaction. However, the encounter overtaking speed in real world practice may not always low. In addition, the importance of the unsteadiness and the nonlinearity for free surface effect should be considered simultaneously in the hydrodynamic interaction investigations. The main challenge of imposing a non-rigid free surface condition arises from the speed term in the body boundary condition with appropriate time-matching scheme. This paper is to propose an iterative time-marching scheme to handle the unsteady and nonlinear free surface boundary condition containing two or more speed terms, and validate its feasibility in investigating the hydrodynamic behaviour of the ships during overtaking operations. A superposition method will be applied to account for the velocity field induced by each vessel with its own and unique speed.

1. Methodology

Considering two vessels denoted as body $\boldsymbol{B}_1$ and body $\boldsymbol{B}_2$ are moving parallel at speed U_1 and U_2 ($U_1 > U_2$). Due to the speed difference, $\boldsymbol{B}_1$ eventually overtakes body $\boldsymbol{B}_1$ A global coordinate system o-xyz is fixed on the earth, and n local coordinate systems o-$x_iy_iz_i$, (i=1, 2, …, n) are fixed on the n-th body. A typical two-body system and the coordinates are shown in Fig. 1. The separation distance and longitudinal distance between body $\boldsymbol{B}_1$ and body $\boldsymbol{B}_2$ are defined as d_t and d_l, respectively. The depth of the water is H. Besides, the velocity potential is time-dependent in the moving frame. It implies the hydrodynamic interaction will be investigated based on the unsteady situation in this section.

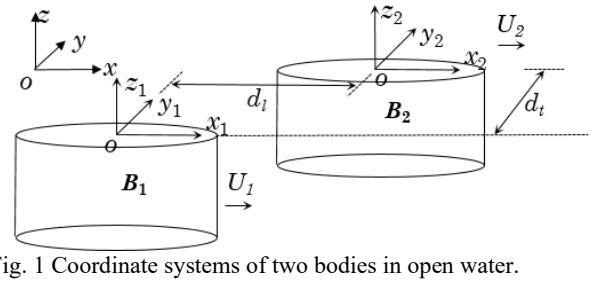

Fig. 1 Coordinate systems of two bodies in open water.

Boundary element method (BEM) is based on the boundary integral partial differential equation to compute the boundary value problem. The advantage of BEM is that it can decrease the computation in 3D into a 2D plane element, which can implement the numerical scheme easily and effectively. $\Phi(x, t)$ is defined as the total velocity potential in the flow domain to describe the disturbance due to the forward motion of the vessels. Assuming the disturbance is small, it represents the total velocity potential produced by the presence of all hulls in the fluid domain in a space-fixed frame to satisfy the following superposition principle:

$$\Phi(\mathbf{x},t)=\sum_{j=1}^{N}\Phi_j(\mathbf{x},t)\ , \quad j = 1, 2, \ldots, N \tag{1}$$

where Φ_j ($\mathbf{x}$, t) is the velocity potential produced by the presence of body $\boldsymbol{B}_\mathbf{j}$ moving with U_j, while the remaining ships are stationary in this frame. The coordinate system fixed in the body $\mathbf{x_j} = (x_j, y_j, z_j)$ (j = 1, 2, …, N) is used to solve the boundary value problem (BVP) for multi-players in concurrent motion. The relation between the body- and the earth-fixed coordinate system is Galilean transformation.

$$x_j = x - U_j t\ , \quad j = 1, 2, \ldots, N \tag{2}$$

Let φ_j ($\mathbf{x_j}$, t) represents Φ_j ($\mathbf{x}$, t) in the body-fixed coordinate system, the following relation can be obtained

$$\frac{d\Phi_j}{dt}=\left(\frac{\partial}{\partial t}-U_j\frac{\partial}{\partial x_j}\right)\varphi_j \tag{3}$$

The velocity potential φ_j satisfies the Laplace equation and body 'exact' boundary condition:

$$\nabla^2\varphi_j(\mathbf{x_j},t)=0, \quad j = 1, 2, \ldots, N \tag{4}$$

$$\frac{\partial\varphi_j}{\partial n}=\delta_{ij}U_j\left(n_x\right)_j \text{, where } i, j = 1, 2, \ldots, N \tag{5}$$

The Kronecker delta δ_{ij} is the quantity defined by

$$\delta_{ij}=\begin{cases}1 & i=j\\ 0 & i\neq j\end{cases} \tag{6}$$

The unsteady nonlinear kinematic and dynamic free surface condition can be written as follows

$$\left(\zeta_j\right)_t-\left(U_j\right)\left(\zeta_j\right)_x+\left(\varphi_j\right)_x\left(\zeta_j\right)_y+\left(\varphi_j\right)_y\left(\zeta_j\right)_z-\left(\varphi_j\right)_z=0\ , \quad \text{on } z=\zeta \tag{7}$$

$$\begin{aligned}&(\varphi_j)_t + g(\zeta_j) - U_j(\varphi_j)_x \\ &-\frac{1}{2}\left[\left((\varphi_j)_x\cdot(\varphi_j)_x\right)+\left((\varphi_j)_y\cdot(\varphi_j)_y\right)+\left((\varphi_j)_z\cdot(\varphi_j)_z\right)\right]=0\end{aligned},$$
on $z=\zeta$ (8)

The boundary condition on the sea bottom and sidewalls can be expressed as

$$\frac{\partial\varphi_j}{\partial n}=0 \tag{9}$$

Besides, a radiation condition is imposed on each control surface to ensure that waves vanish at infinity

$$\varphi_j \to 0,\quad \zeta_j \to 0 \quad as\ \sqrt{x_j^2+y_j^2}\to\infty \tag{10}$$

Equation. (1)-(10) forms a completed set of BVP. Here, only a single speed of ship j appears in the free surface condition in Equation. (7)-(8), and the coupled problem is decoupled into N independent sets of BVPs. The unsteady free surface boundary condition will be investigated in the time domain by an iteration scheme. Once the unknown potential φ_j is solved, the unsteady pressure components under its individual coordinate system can be obtained from linearized Bernoulli's equation

$$p_j\big|_{\mathbf{x_j}} = -\rho\left[\frac{\partial\varphi_j}{\partial t}\Big|_{\mathbf{x_j}} - U_j\frac{\partial\varphi_j}{\partial x_j}\Big|_{\mathbf{x_j}}\right] \quad ,j = 1, 2\ldots N \tag{11}$$

Due to the first unsteady term in Equation.(11), the total pressure P_j in the coordinate system $\mathbf{x_j}$ cannot be expressed directly as the sum of all the pressure components in each local frame. To transfer the pressure from the coordinate system $\mathbf{x_i}$ to $\mathbf{x_j}$, the following relation can be obtained

$$\frac{d\varphi_i}{dt}\Big|_{\mathbf{x_j}} = \left(\frac{\partial}{\partial t} - (U_j - U_i)\frac{\partial}{\partial x_i}\right)\varphi_i\Big|_{\mathbf{x_j}} \tag{12}$$

It should be noted that the partial derivative symbol of the first term in Equation. (11) is retained to make it consistent with Equation. (3) where the potential is expressed in the body-fixed coordinate system$\mathbf{x_j}$. However, here the body-fixed coordinate system $\mathbf{x_j}$ turns to be the reference frame for the other body-fixed coordinate system $\mathbf{x_i}$. Therefore, $\frac{\partial\varphi_j}{\partial t}$ is actually calculated as a total derivative by using Equation. (12). The unsteady pressure in the coordinate system $\mathbf{x_i}$ ($i = 1, 2, \ldots, N \quad i\neq j$) can then be transferred to $\mathbf{x_j}$ as

$$\begin{aligned}p_i\big|_{\mathbf{x_j}} &= -\rho\left[\left(\frac{\partial}{\partial t} - (U_j - U_i)\frac{\partial}{\partial x_i}\right)\varphi_i\Big|_{\mathbf{x_j}} - U_i\frac{\partial\varphi_i}{\partial x_i}\Big|_{\mathbf{x_j}}\right] \\ &= -\rho\left(\frac{\partial}{\partial t} - U_j\frac{\partial}{\partial x_i}\right)\varphi_i\Big|_{\mathbf{x_j}}\end{aligned} \tag{13}$$

The total pressure P_j in the coordinate system $\mathbf{x_j}$ can be written as

$$P_j\big|_{\mathbf{x_j}} = \sum_{i=1}^{N} p_i\big|_{\mathbf{x_j}} = -\rho\sum_{i=1}^{N}\left(\frac{\partial}{\partial t} - U_j\frac{\partial}{\partial x_i}\right)\varphi_i\Big|_{\mathbf{x_j}} \tag{14}$$

Integral the pressure over the hull surface, the forces (or moments) can be obtained by

$$F_i^j = \iint_{S_j} pn_i ds \tag{15}$$

where i = 1, 2, …, 6, representing the force in surge, sway, heave, roll, pitch and yaw directions, and

$$n_i = \begin{cases} n, & i = 1,2,3 \\ x\times n, & i = 4,5,6 \end{cases} \tag{16}$$

2. Discretization of free surface condition

The novel numerical method has been developed to simulate the unsteady interaction problem between two ships. It should be noted that this new algorithm needs to be implemented in different local reference in the body $\boldsymbol{B_1}$ or body $\boldsymbol{B_2}$, respectively. To determine the initial condition at t = 0, we assume that at the initial stage of ship-to-ship operation, the moving ships are sufficiently far apart so that their interactions are negligible. Thus, the time-dependent non-linearized free surface condition in Equation. (7)-(8) are linearized to the steady linearized free surface condition [20] in the body-fixed coordinate system can be obtained

$$U_j^2\frac{\partial^2\phi_j}{\partial x_j^2} + g\frac{\partial\phi_j}{\partial z_j} = 0 \text{ , on } z = 0, \tag{17}$$

where the subscript j indicates the index of the ship. The time derivatives in the free surface condition have to be discretized. The three-time-level scheme is used to obtain the first derivatives of φ_j and ζ_j.

At each iterative step k, the linear terms of x--derivative in Equation. (18) are approximated implicitly on the left-hand side (LHS) terms. The rest nonlinear terms and cross-derivatives are put on the right-hand sides (RHS) as the knowns for the next

iteration $t = t_{n+1}$ to update the wave elevation. The dynamic condition in equation (18) is then satisfied through an implicit method using the present solution in Equation. (19)to update potential φ_j. All variables are then updated by the latest values from the iteration. Residual errors of time derivatives of $\left|(\varphi_j^{n+1,k})^* - \varphi_j^{n+1,k}\right|$ & $\left|(\zeta_j^{n+1,k})^* - \zeta_j^{n+1,k}\right|$can be evaluated. If both the $\left|(\varphi_j^{n+1,k})^* - \varphi_j^{n+1,k}\right| < \varepsilon$ and $\left|(\zeta_j^{n+1,k})^* - \zeta_j^{n+1,k}\right| < \varepsilon$, the iteration stops and $\varphi_j^{n+1,k}$ and $\zeta_j^{n+1,k}$ will be used to calculated the pressure. Otherwise, $(\varphi_z)_j^{n,k}$in Equation. (18) will be calculated by $\varphi_j^{n+1,k}$. It is known that the iterative scheme has advantages of high accuracy and good numerical stability. At each iterative step k,

$$\frac{3\zeta_j^{n+1,k} - 4\zeta_j^n + \zeta_j^{n-1}}{2\Delta t} - U\cdot(\zeta_x)_j^{n+1,k} = -(\varphi_x)_j^n\cdot(\zeta_x)_j^n - (\varphi_y)_j^n\cdot(\zeta_y)_j^n + (\varphi_z)_j^n \tag{18}$$

$$\frac{3\varphi_j^{n+1,k} - 4\varphi_j^n + \varphi_j^{n-1}}{2\Delta t} - U\cdot(\varphi_x)_j^{n+1,k} = -g\cdot\zeta_j^{n+1,k} - \frac{1}{2}\left[(\varphi_x\cdot\varphi_x)_j^{n,k} + (\varphi_y\cdot\varphi_y)_j^{n,k} + (\varphi_z\cdot\varphi_z)_j^{n,k}\right] \tag{19}$$

In which $\varphi_j^{n+1,k}$ and $\zeta_j^{n+1,k}$ are the predicted values of $\varphi_j^{n,k}$ and $\zeta_j^{n,k}$ after the kth iteration. In order to obtain more stable numerical results, the 2nd-order up-wind difference scheme was implemented to obtain the spatial derivatives of the φ_x and ζ_x on the LHS of the Equation (18)-(19)[21]. The transverse derivatives and the vertical derivatives of the nonlinear items are evaluated by using a central difference scheme. The implicit scheme is unconditionally stable, and its temporal and spatial accuracy is of second order, i.e., O (Δt^2), O ($\Delta x^2, \Delta y^2$). Once the unknown potential $\varphi_j\big|_{x_j}$ is solved, the $\varphi_i\big|_{x_j}$ simulated in the other body reference ***i*** will calculated based on the steady linear FSBC. It is because of the position of the elements distributed on the free surface is only fixed to the body reference j. Calculating the changing free surface in the reference i is very complicated. The unsteady pressure components under its individual coordinate system can be obtained from linearized Bernoulli's Equation. (14). The wave elevation on the free surface can be obtained from dynamic free-surface boundary condition in Equation. (8). Similar to the pressure expression, the total wave elevation can be written as

$$\zeta\big|_{\mathbf{x_j}} = -\rho\sum_{i=1}^{N}\left(\frac{\partial}{\partial t} - U_j\frac{\partial}{\partial x_i}\right)\phi_i\big|_{\mathbf{x_j}} \tag{20}$$

3. Result and discussion

3.1 *Validation tests*

Two Cylindroids on passing test

Model-test data on the ship-to-ship interaction with different speeds is rather rare. To validate the developed numerical method, firstly, two identical cylindroids model in overtaking is simulated. Fig. 2 is the mesh distribution on the partial computational domain when Model $\boldsymbol{C_1}$ **is** overtaking Model $\boldsymbol{C_2}$. It should be noted that the sidewalls of the tank are not modelled and the longitudinal separation d_l is measured in the body-fixed frame on Model $\boldsymbol{C_1}$. The main particulars of Model $\boldsymbol{C_1}$ can be found in Table 1.

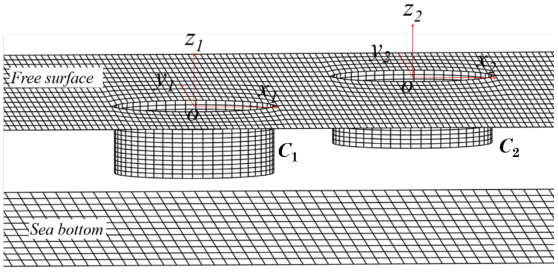

Fig. 2 Panel distribution on the computation domain of two identical cylindroids model in overtaking on the sea bottom. There are in total 4544 panels distributed on the total computation domain in this simulation: 2222 panels distributed on the free surface SF, 782 on each wetted body surface S_H and 756 on the sea bottom S_B. The computational domain is truncated at 2L upstream, 2L downstream and 0.25L sideways with regard to the body-fixed reference frame.

Table 1 Parameters of the cylindroids

Dimension	Value
Length (m)	0.8
Breadth (m)	0.1
Draft (m)	1.47

The numerical results, comparing with the experimental measurements, are shown in Fig. 3. shows the interaction forces (*a*) The wave-resistance, (*b*) the sway force and (*c*) the yaw moment on Model $\boldsymbol{C_2}$ at $F_n = 0$ passed by Model $\boldsymbol{C_1}$ at $F_n = 0.217$ at the water depth H = 3 m. Generally, the agreement between present potential flow solver and experimental measurement is very satisfied. It indicates the developed numerical algorithm is applicable to predict the hydrodynamic interactions between two ships with different forward speeds. It should be noted that it also compares the nonlinear free surface condition with the linear free surface condition. The results indicate that the nonlinear term in this passing problem is not very important under

such overtaking speed. Therefore, it will be neglect in the following simulations.

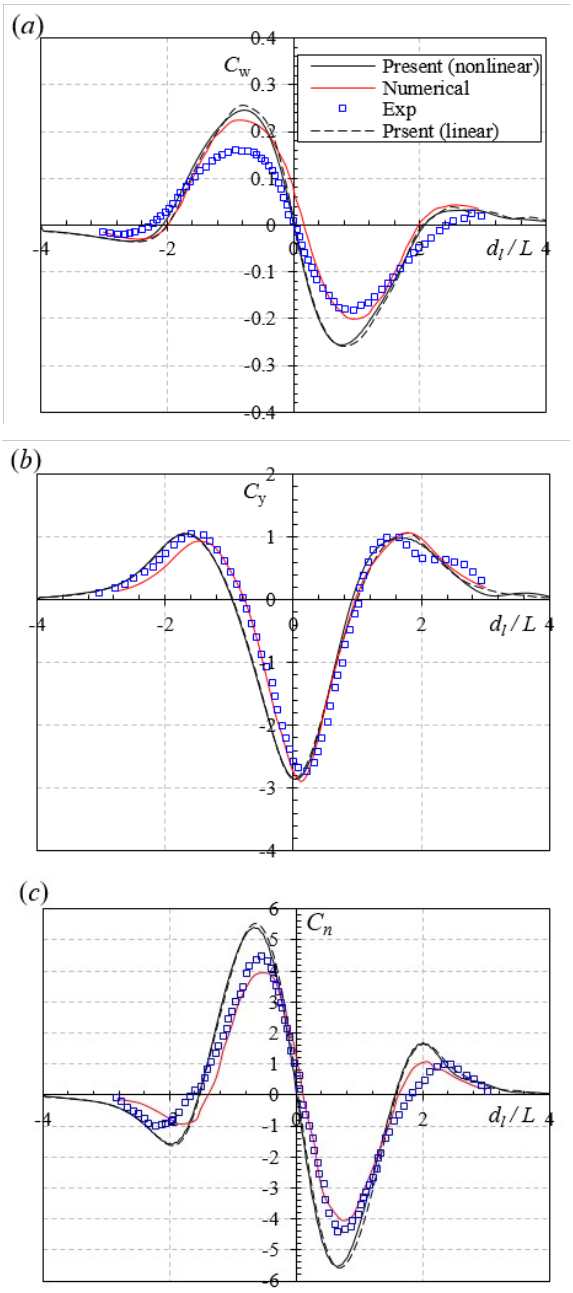

Fig. 3 (*a*) The wave-resistance, (*b*) the sway force and (*c*) the yaw moment on $\boldsymbol{C_2}$ at the $F_n = 0$ passed by $\boldsymbol{C_1}$ at the $F_n = 0.217$. The water depth $H = 3$ m and the separation distance is $d_t = 5.0B$. The positive d_l values denote that $\boldsymbol{C_1}$ is on the upstream side of $\boldsymbol{C_2}$. As $\boldsymbol{C_1}$ moves to the down-stream side, d_l becomes negative. EFD results are published by Oltmann[22]and the numerical results are calculated by the Xu[8].

Wigley III hulls tests

To validate the effectiveness of the present numerical simulation method, two typical conditions of passing and overtaking cases of Wigley hulls in open water are investigated, and the calculated results of hydrodynamic interaction forces are compared with the corresponding results obtained by the slender-body theory or RANS-based CFD method. Fig. 4 shows the panel distribution on the computation domain of two identical Wigley III hulls during the overtaking.

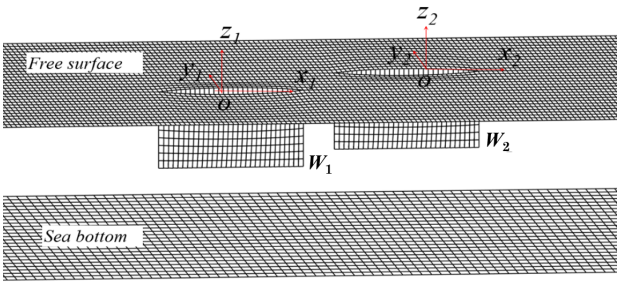

Fig. 4 Panel distribution on the computation domain of two identical Wigley III hulls in overtaking on the sea bottom. There are in total 4544 panels distributed on the total computation domain in this simulation: 2222 panels distributed on the free surface S_F, 782 on each wetted body surface S_H and 756 on the sea bottom S_B. The computational domain is truncated at 2L upstream, 2L downstream and 0.25L sideways with regard to the body-fixed reference frame.

Table.2. Principal dimensions of the Wigley III model

Dimensions Item	Value
Length (m)	3.0
Breadth (m)	0.3
Draft (m)	0.1875

In Fig. 5, the present numerical results are compared with those obtained by using the slender-body theory by Tuck[4] and the high-order numerical results by the Xu[8] for a ship $\boldsymbol{W_1}$ passing by a berthed ship $\boldsymbol{W_2}$ in unrestricted water. It can be seen that the hydrodynamic interaction forces obtained by the present method agree well with those by using the slender-body theory.

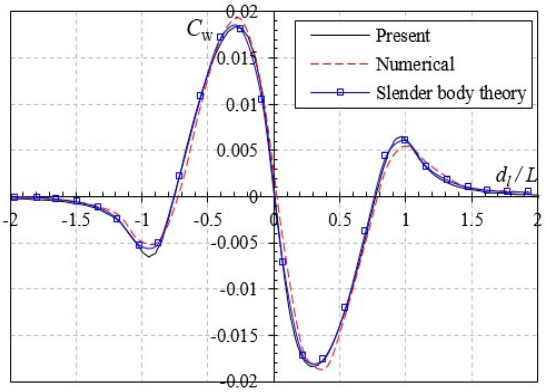

(*a*)

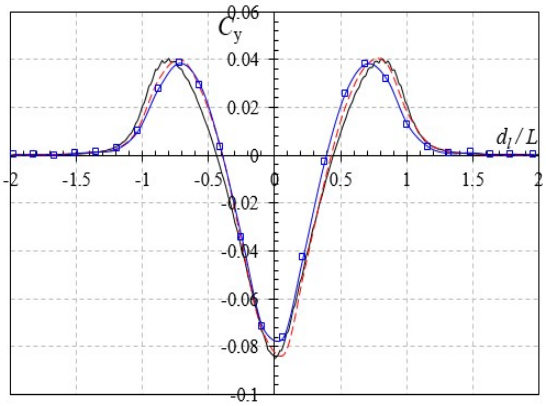

(*b*)

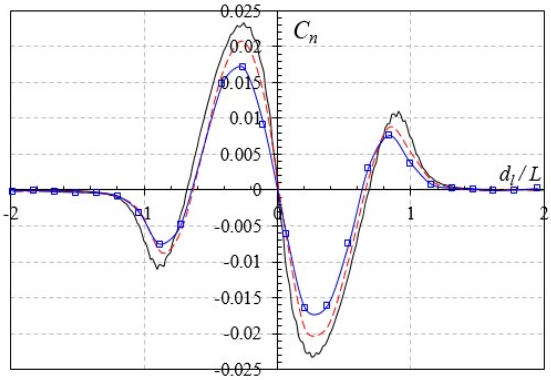

(*c*)

Fig. 5 (*a*) The wave-resistance, (*b*) the sway force and (*c*) the yaw moment on $\boldsymbol{W_2}$ at the $F_n = 0$ passed by $\boldsymbol{W_1}$ at the $F_n = 0.066$. The separation distance is d_t = 1.5 B and the water depth is infinite. The positive d_l values denote that $\boldsymbol{W_1}$ is in the upstream side of $\boldsymbol{W_2}$. As $\boldsymbol{W_1}$ moves to the down-stream side, d_l becomes negative. EFD results are published by slender body theory by Tuck[4] and the numerical results are calculated by Xu[8].

3.2 *Overtaking tests*

Fig. 6 shows the comparison of the presented interactions forces on Model $\boldsymbol{W_2}$ at the F_n = 0.02 overtaken by $\boldsymbol{W_1}$ at the F_n = 0.066 with the numerical results by Xu[8]. The separation distance is d_t = 2.0B and the water depth H / D =1.5. The negative values shown in Fig. 6. (a) represent the resistance that is opposite to the moving direction, while the positive values represent a thrust, which is the same as the moving direction. An interesting finding is that a very large thrust force is observed at d_l / L = -0.5 during the passing and overtaking maneuvering. The thrust force is observed at d_l / L_E = 0.5, where the bow of $\boldsymbol{W_1}$ approaches the midship of $\boldsymbol{W_2}$ longitudinally. It can be explained that before overtaking (-1 < d_l / L < 0), the presence of faster ship ($\boldsymbol{W_1}$) accelerates the fluid velocity around the stern area of $\boldsymbol{W_2}$. As a result, the pressure distributed over ship stern decreases. At the same time, the pressure distributed over the ship bow retains the same level. Increased resistance is expected by pressure integral over the hull surface of $\boldsymbol{W_2}$. After overtaking (0 < d_l / L < 1), the high-pressure area transfers to the ship bow, which will correspondingly lead to a propulsion force. There are some empirical formulas established to solve the interaction moment based on these peaks. However, as those peaks are not predictable, the applicability of those empirical formulas is very limited. It has been found that in the ship-bank and ship-lock problem, the potential flow method fails to predict the sign of yaw moment due to the weak lifting force caused by the cross-flow in the stern[23]. However, for the unsteady interaction problem between the ships, the hydrodynamic interaction is much more important than cross-flow effects. The predictions of yaw moment by a potential flow solver are therefore reliable.

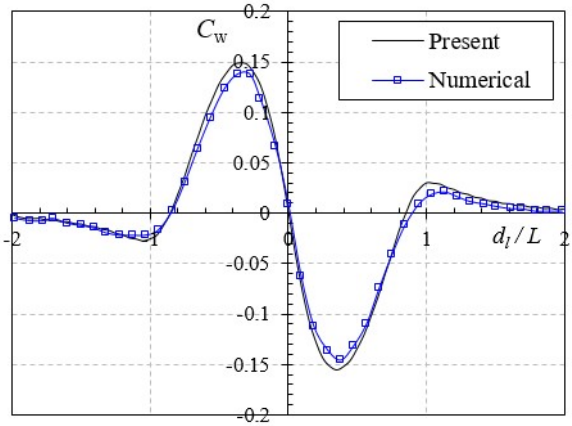

(*a*)

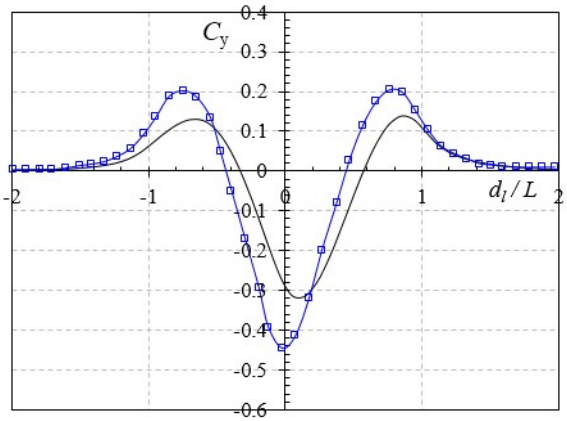

(*b*)

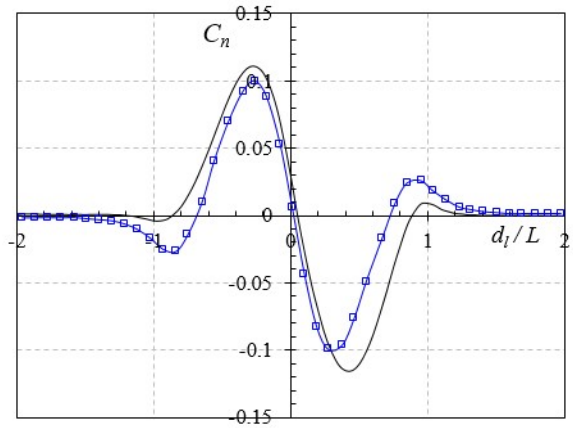

(*c*)

Fig. 6 (a) The wave-resistance, (b) the sway force and (c) the yaw moment on W_2 at the F_n = 0.02 overtaken by W_1 at the F_n = 0.066. The separation distance is d_t = 2.0 B and the water depth H /D =1.5. The numerical results are calculated by Xu[8].

3.3 *Parametric study*

a. Different ratios of ship speeds

After validations, the present numerical algorithm with the superposition method can then be extended to investigate the effect of the speed, separation distance and water depth. Firstly, to examine the effect of the changing speed ratio $\gamma = U_1/U_2$, computations of overtaking manoeuvers are carried out with F_{n2} = 0.066, while the value of F_{n1} changes between 0.1 and 0.165. The water depth is H/D =1.5. In Fig. 7 (*a*), the normalized longitudinal forces on the W_2 versus increasing instantaneous stagger of various ratio γ can be seen. Meanwhile, In Fig. 7, the forces/moments acting on the W_2 at higher ratio γ exhibit much more variations than the cases with lower γ after the overtaking taken place (d_l/L >1.0). At this position, W_2 higher is maneuvering to the W_2 's wake region, the free surface effect in the far-field then can be observed. Besides, the peaks induced by far-field waves are unpredictable. Therefore, the empirical formulas based on low-speed model[24-26] is not applicable to predict the interaction forces when the free surface effect becomes important.

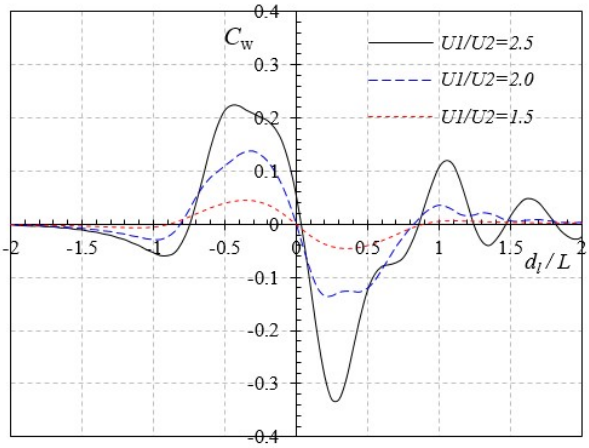

(*a*)

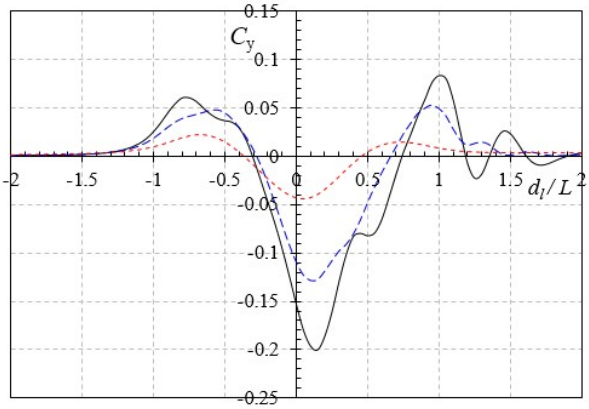

(*b*)

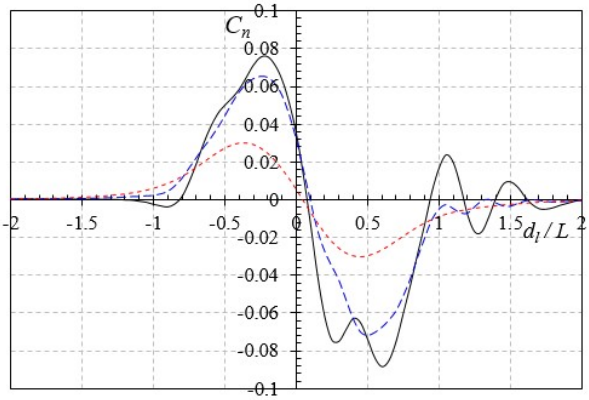

(*c*)

Fig. 7 (*a*) The wave-resistance, (*b*) the sway force and (*c*) the yaw moment are acting on W_2 at different ratios of ship speeds during overtaking. The separation distance is d_t = 2.0 *B* in *H*/*D* =1.5.

b. Different separation distance d_t between two ships

The influence factor of the lateral distance d_t between the hulls also plays a crucial role in hydrodynamic interaction. To analyse and reveal the influences of these factors, a series of calculations are carried out for two vessels in overtaking conditions. The constant speed ratio is $\gamma = U_1/U_2$ = 2.0. The calculations are conducted for d_t = 2.0*B*, 2.5*B*, 3.0*B*. The water depth

is kept unchanged. Fig. 8 shows the calculation results of the hydrodynamic interaction forces and yaw moment acting on $\boldsymbol{W_2}$. It can be seen that the changing tendency is the same for different d_t. The longitudinal force experiences consecutive decrease and increase. The lateral force is distinguished by initial repulsion, followed by attraction and repulsion again. The yaw moment is characterized by four phases, that is, consecutive bow attraction and bow repulsion. It should be noted that the main difference occurs at the peak points in each curve. These figures reveal that the separation distance between two hulls plays an important role in hydrodynamic interaction, and the magnitudes of the hydrodynamic interaction force and moment decrease with the increase of the lateral distance.

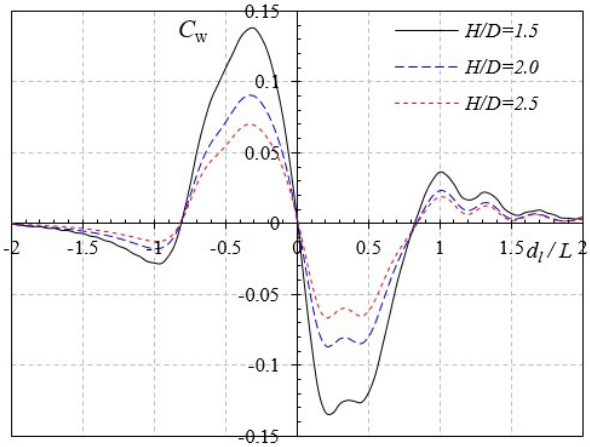

(*a*)

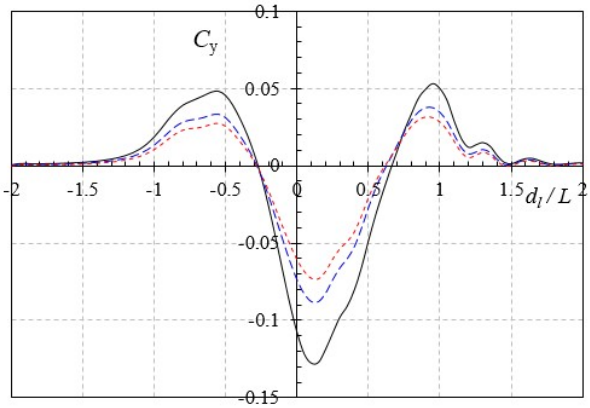

(*b*)

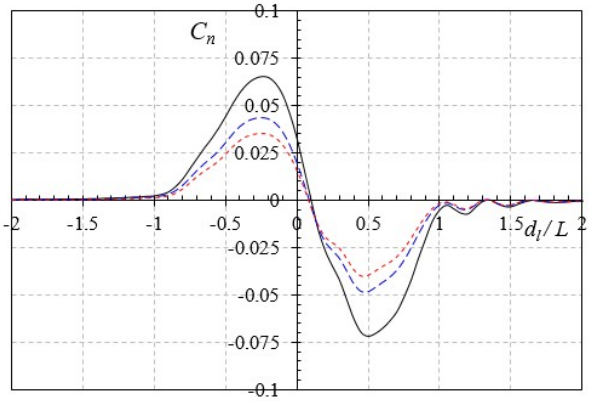

(*c*)

Fig. 8 (*a*) The wave-resistance, (*b*) the sway force and (*c*) the yaw moment acing on $\boldsymbol{W_2}$ at different separation distance during overtaking. The speed radio is $\gamma=U_1/U_2=2.0$ and the $H/D=1.5$.

c. Different water depth *H/D*

To investigate the influence of water depth *H/D* on the hydrodynamic interaction forces of two ships in overtaking conditions, the calculations are conducted for different ratios of water depth to draught *H/D* = 1.5, 2.0 and 2.5. The lateral distance between the vessels is $d_t = 2.0B$, and the ratio of the $\gamma=U_1/U_2=2.0$ is kept unchanged. Fig. 9 shows the hydrodynamic interaction forces and yaw moment acting on $\boldsymbol{W_2}$. From the figures, it can be seen that the effect of the water depth on hydrodynamic interaction forces and yaw moment are almost the same as the effect of the separation distance. It reveals that when the ships are in the overtaking process in the restricted waterways, the peak magnitude of the hydrodynamic interaction forces would be amplified.

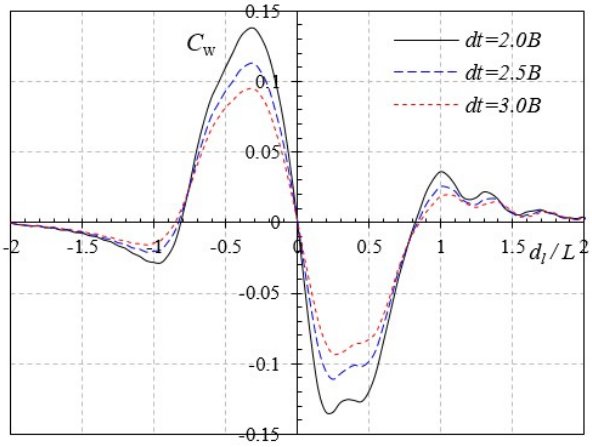

(*a*)

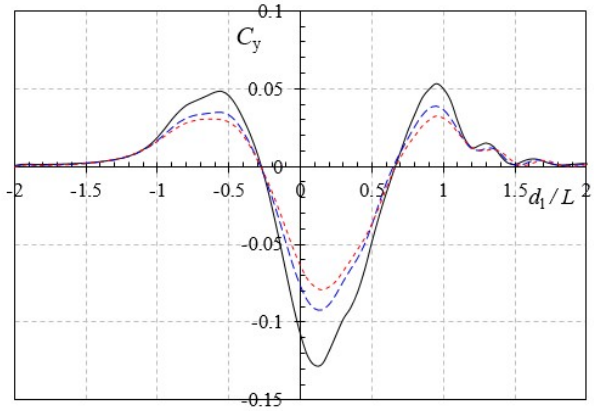

(*b*)

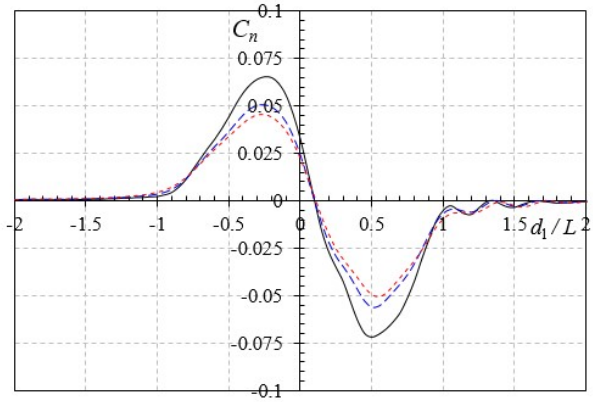

(*c*)

Fig. 9 (*a*) The wave-resistance, (*b*) the sway force and (*c*) the yaw moment acing on W_2 at different water depth ratios during overtaking. The separation distance is d_t = 2.0 *B* and the γ=U_1/U_2 = 2.0.

3.4 *Wave patterns generated by the two ships in deep water*

In this study, another important objective is to obtain the wave patterns, and to observe the interference between two sets of ship waves during the overtaking maneuvers. As mentioned before, the free surface effect should not be neglected at γ > 0.2, such that it would investigate the Froude number of the W_1 keeps constant F_{n1} = 0.3, while the value of the ratio in the changes of γ=U_1/U_2 = 1.2, 1.5 and 2.0. The numerical results of moralized forces/moment at different values γ are depicted in Fig. 10.

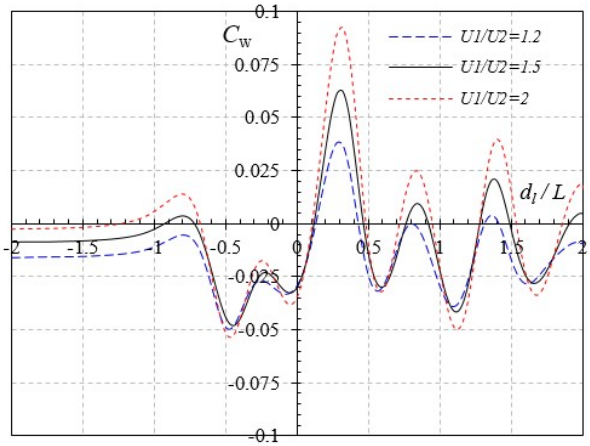

(*a*)

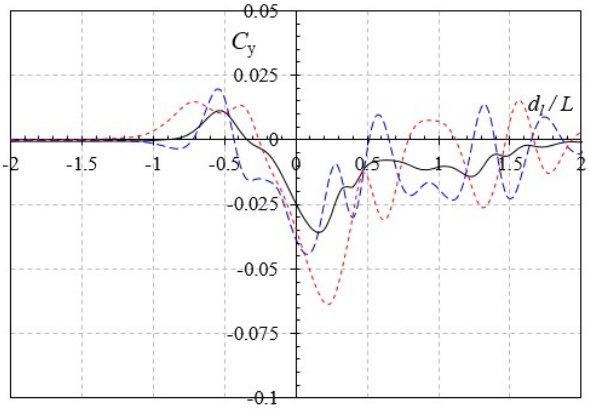

(*b*)

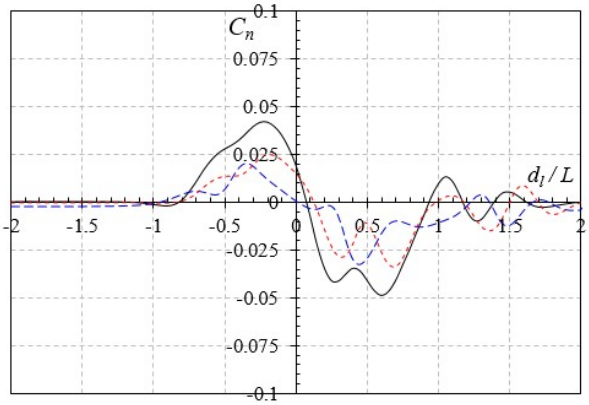

(*c*)

Fig. 10 Hydrodynamic force and moment acing on W_2 at different ratios of ship speeds during overtaking. The separation distance is d_t = 2.0 *B* and the water depth is infinite.

The coefficient curves exhibit distinct fluctuations when the W_1 overtakes towards the W_2 from -2*L* to 2*L* downstream. The amplitude of the fluctuations becomes larger as the W_1 gets closer to the W_2. As the radio γ increases, the sway force coefficient C_y and the yaw moment coefficient C_n acting on W_2 with different values γ show insignificant differences in fluctuation phase, while the wave-making resistance C_w keeps the same

fluctuation phase.

In order to find how the wave patterns alter the hydrodynamic interaction, we depict the wave flows around the ships at various d_l/L. The instantaneous wave patterns between the ships at various γ during the overtaking process with different configurations are shown in Fig. 11. It should be noted that the total wave elevation ζ presented is not only the simple superposition of the waves generated by two individual hulls moving forward. When we calculate the wave elevation produced by $\boldsymbol{W_1}$, the presence of $\boldsymbol{W_1}$ is also considered. Typically, $\boldsymbol{W_1}$ is treated as an obstacle, which is momentarily stationary in the body-fixed frame of $\boldsymbol{W_1}$. Therefore, the diffraction and reflection by $\boldsymbol{W_1}$ are considered in the present study. The first significant disturbance occurs when the d_l/L = -0.5 corresponding to Fig. 11(*a*), (*e*) and (*i*). The stern of $\boldsymbol{W_2}$ locates at the divergent wave of $\boldsymbol{W_1}$ experience larger hydrodynamic forces and moment. For example, in Fig. 11(*a*), if the starboard of $\boldsymbol{W_2}$'s aft part is in the wave trough, an extra resistance will be added. These reflected waves can be seen clearly when the two ships are in the close stagger position around the d_l/L = 0.3 in Fig. 11(*c*), (*g*) and (*k*). It can be seen that a significant increase in wave elevations is observed in the gap between hulls. When $\boldsymbol{W_2}$ is overtaken by $\boldsymbol{W_1}$, the starboard of $\boldsymbol{W_2}$'s fore part is in the wave trough region. As a result, the wave resistance is decreasing. With smaller γ as shown in Fig. 11 (*e*)-(*i*), $\boldsymbol{W_2}$ moves at much slower speeds than the overtaking $\boldsymbol{W_1}$ generates insignificant waves; therefore, its wave patterns are almost imperceptible in comparison with those of $\boldsymbol{W_2}$. As the value of γ keeps decreasing, two hulls generate waves with different amplitudes and wavelengths. As a result, less wave interference is observed, which does not change the wave elevation of the flow field. However, regardless of the values of γ, the free surface on the port of the $\boldsymbol{W_1}$ is less disturbed by the influence of $\boldsymbol{W_2}$ during the overtaking process. It can be explained also from the wave energy theory. When the $\boldsymbol{W_2}$ is wholly or partly in the divergent disturbance region generated by the $\boldsymbol{W_1}$, the interaction becomes significant. The bow and stern waves interfere in this region, and the wave energy concentrated in this region is usually high, especially when the shipping speed is moderate or high.

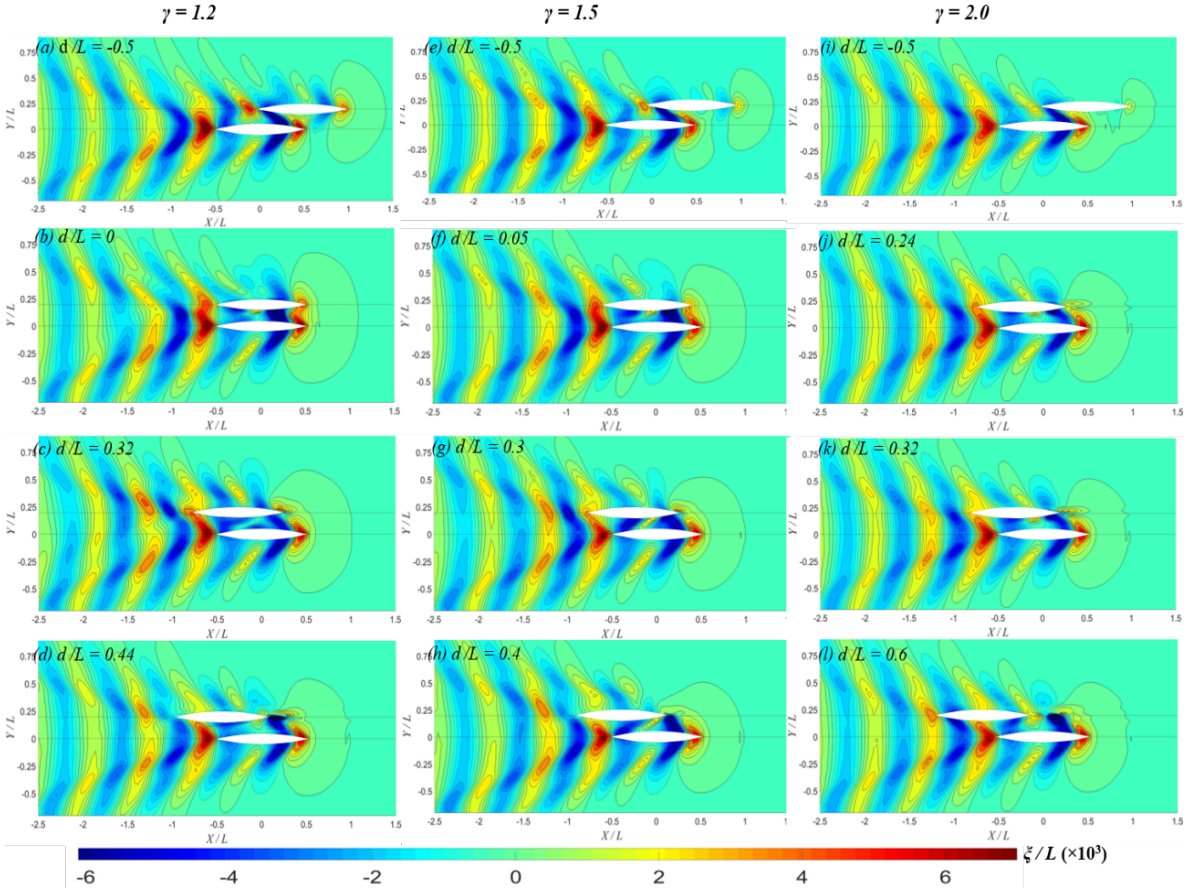

Fig. 11 The wave pattern of the vessel $\boldsymbol{W_2}$ at different ratios γ during overtaking at the different position corresponding to the vessel $\boldsymbol{W_1}$. The separation distance is d_l = 2.0 B and the water depth is infinite.

4. Conclusions

In the present study, the unsteady potential flow solver

is extended to investigate the unsteady phenomenon of the interaction between the ships in shallow water. By imposing an unsteady non-linear free surface condition to the BVP, we successfully captured the unsteady waves initiated by ships during overtaking process. The results of the potential-flow panel method are validated by the experimental data and the high-order panel method. The main features of the hydrodynamic interaction in the overtaking process, e.g., the maximum lateral force and the associated instantaneous stagger, are satisfactorily captured by the current computational model with restrained sinkage and trim. When the speed radio between ships becomes large, it is shown that the ship overtaken by the drafter experiences loads of larger magnitude and violet oscillations. It can also be observed that with the small speed radio, the forces/moment of both ships approaches those of a steady-state di-hull system. In conclusion, the unsteady free surface around hulls is found to have non-negligible effects on the forces acting on the ships. On one hand, the present of the slower ship effectively blocks the waves generated by the fast overtaking counterpart. On the other hand, when the ships travel with comparable speeds, the wave interference considerably changes the free surface elevations between the two ships.

References

[1.] Varyani, K.S., R.e. McGregor, and P. Wold, *Interactive forces and moments between several ships meeting in confined waters.* Control Engineering Practice, 1998. **6**(5): p. 635-642.

[2.] Kijima, K. and H. Yasukawa, *Manoeuvrability of ships in narrow waterway.* Journal of the Society of Naval Architects of Japan, 1984(156): p. 171-179.

[3.] Yeung, R.W., *On the interactions of slender ships in shallow water.* Journal of Fluid Mechanics, 1978. **85**(1): p. 143-159.

[4.] Tuck, E.O. and J.N. Newman. *Hydrodynamic interactions between ships*. in *Symposium on Naval Hydrodynamics, 10th, Proceeding, Pap and Discuss,* . 1976. Cambridge, Mass,.

[5.] Dand, I.W. *Some aspects of tug-ship interaction*. in *International Tug Convention (4th)*. 1975. New Orleans, .

[6.] Tuck, E.O., *Shallow-water flows past slender bodies.* Journal of Fluid Mechanics, 1966. **26**(1): p. 81-95.

[7.] Korsmeyer, F.T., C.H. Lee, and J.N. Newman, *Computation of ship interaction forces in restricted waters.* Journal of Ship Research, 1993. **37**(04): p. 298-306.

[8.] Xu, H.F., et al., *Unsteady hydrodynamic interaction between two cylindroids in shallow water based on high-order panel method.* Engineering Analysis with Boundary Elements, 2016. **70**: p. 134-146.

[9.] Zhou, X., S. Sutulo, and C.G. Soares, *Computation of ship hydrodynamic interaction forces in restricted waters using potential theory.* Journal of Marine Science and Application, 2012. **11**(3): p. 265-275.

[10.] Xiang, X. and O.M. Faltinsen, *Maneuvering of Two Interacting Ships in Calm Water.* Marine Systems & Ocean Technology, 2010. **1**(2).

[11.] Söding, H. and F. Conrad, *Analysis of Overtaking Manoeuvres in a Narrow Waterway.* Ship Technology Research, 2005. **52**(4): p. 189-193.

[12.] Duan, W.Y., et al., *Comparison research of ship-to-ship hydrodynamic interaction in restricted water between TEBEM and other computational method.* Ocean Engineering, 2020. **202**: p. 107168.

[13.] Yuan, Z.M., et al., *Steady hydrodynamic interaction between human swimmers.* Journal of the Royal Society Interface, 2019. **16**(150): p. 20180768.

[14.] Yuan, Z.M., L. Li, and R.W. Yeung, *Free-surface effects on interaction of multiple ships moving at different speeds.* Journal of Ship Research, 2019. **63**(4): p. 251-267.

[15.] Yuan, Z.M., *Ship hydrodynamics in confined waterways.* Journal of Ship Research, 2019. **63**(1): p. 16-29.

[16.] Ren, H.L., et al., *A Numerical Method for Calculation of Ship–Ship Hydrodynamics Interaction in Shallow Water Accounting for Sinkage and Trim.* Journal of Offshore Mechanics and Arctic Engineering, 2020. **142**(5).

[17.] Zou, L. and L. Larsson, *Numerical predictions of ship-to-ship interaction in shallow water.* Ocean Engineering, 2013. **72**: p. 386-402.

[18.] Mousaviraad, S.M., S.H. Sadat-Hosseini, and F. Stern, *Ship–ship interactions in calm water and waves. Part 1: analysis of the experimental data.* Ocean Engineering, 2016. **111**: p. 615-626.

[19.] Zhou, L.L., H.S. Abdelwahab, and S.C. Guedes, *Experimental and CFD investigation of the effects of a high-speed passing ship on a moored container ship.* Ocean Engineering, 2021. **228**.

[20.] Newman, J.N., *Marine hydrodynamics*. 1977: MIT press.

[21.] Kring, D.C., *Time domain ship motions by a three-dimensional Rankine panel method.* PhD Thesis, 1994.

[22.] Oltmann, P., *Experimentelle untersuchung der hydrodynamischen wechselwirkung schiffsähnlicher körper.* Schiff Hafen, 1970. **22**: p. 701-709.

[23.] Yuan, Z.M., et al., *Hydrodynamic interactions between two ships travelling or stationary in*

shallow waters. Ocean Engineering, 2015. **108**: p. 620-635.

[24.] Vantorre, M., E. Verzhbitskaya, and E. Laforce, *Model test based formulations of ship–ship interaction forces.* Ship Technology Research, 2002. **49**: p. 124-141.

[25.] Varyani, K.S., R. McGregor, and P. Wold, *Identification of trends in extremes of sway–yaw interference for several ships meeting in restricted waters.* Ship Technology Research, 2002. **49**: p. 174-191.

[26.] Lataire, E., et al., *Mathematical modelling of forces acting on ships during lightering operations.* Ocean Engineering, 2012. **55**: p. 101-115.